AIAA JOURNAL
Vol. 39, No. 12, December 2001

Drag Coefficient Reduction in the Presence of Pressure Gradients by Heat Transfer

C. Feiler*
85614 Munich/Kirchseeon, Germany

Heat transfer is known to affect the surface shear stress of boundary layers. An attempt is being made to investigate the behavior of coupled compressible boundary layers of air in the presence of pressure gradients around airfoil shapes with the aid of numerical simulation and to minimize the drag coefficient by an optimized distribution of surface heating and cooling. The obtained results indicate that a distinct reduction of the drag coefficient can be achieved by moderate values of surface heat fluxes. Some consideration of the freestream velocity dependence and the effect of heat transfer on the transition location is included, as well as the effect of different airfoil geometries. Two illustrative examples are presented.

Nomenclature

A	=	area, m^2
C	=	Chapman–Rubesin viscosity parameter
C_p	=	pressure coefficient
c	=	chord length, m
c_d	=	drag coefficient
c_f	=	skin-friction coefficient
c_{ht}	=	empirical thermal drag reduction factor
Fr_c	=	Frossling number based on chord
i	=	imaginary part
M	=	Mach number
m	=	pressure gradient parameter
Pr	=	Prandtl number
p	=	pressure, Pa, bar
q_w	=	wall heat rate, W
$q_{w,\mathrm{abs}}$	=	positive signed wall heat rate, W
q''_w	=	wall heat flux, W/m^2
Re	=	Reynolds number based on subscript
St	=	Stanton number
St_t	=	unheated starting length Stanton number
T	=	temperature, K
u_e	=	external velocity, m/s
u_0	=	initial velocity, m/s
W_d	=	drag work, W
x_s, s	=	surface distance, m
x_{tr}	=	location, where transition starts (indifference location), m
α	=	amplification factor, −
α_i	=	angle of incidence, deg
δ	=	boundary-layer thickness, m
η	=	similar boundary-layer y-distance
η_{th}	=	thermal efficiency, %
Θ	=	momentum thickness, m
μ	=	viscosity, kg/m · s
$\tilde{\mu}$	=	viscosity to freestream viscosity ratio
ρ	=	density, kg/m^3
τ_w	=	surface shear stress, N/m^2
ϕ	=	disturbance amplitude, m
ω	=	dimensionless disturbance frequency

Received 6 January 2000; revision received 14 September 2000; accepted for publication 27 April 2001.

*Engineer; currently Research Assistant, Chair for Combustion Engines and Flight Propulsion, Brandenburg Technical University, 03044 Cottbus, Germany.

I. Introduction

THE behavior of coupled boundary layers with varying pressure gradients in the presence of nonzero heat transfer has been widely investigated. An investigation of the behavior of airfoil boundary layers in the presence of heat transfer and pressure gradients has been presented by Morduchow and Grape.[1] This contribution is based on integral methods and also covers boundary-layer stability. A theoretical investigation of the generation of thrust by heating in subsonic and supersonic ideal flows has been presented by Oswatitsch.[2] This study shows how heat sources placed in the freestream affect the ideal flow pressure distribution, and it is found, that for $M < 1$, placing heat sources in the retardation regions of airfoil-like geometries generates thrust. Subsequently, Feltgen[3] has conducted experiments by externally burning hydrogen gas in the retardation regions at the tip and at the trailing edge. These investigations do not account for boundary-layer effects. Numerical calculation methods and a thorough treatment of coupled boundary layer flows have been presented, for example, by Cebeci and Bradshaw.[4] Numerous comparisons with experimental data have been included.

II. Boundary Layers in the Presence of Pressure Gradients and Heat Transfer

The local skin-friction coefficient c_f and the wall shear stress τ_w are defined as

$$c_f = \frac{\tau_w}{0.5\rho_e u_e^2}, \qquad \tau_w = \mu \left.\frac{\mathrm{d}u}{\mathrm{d}y}\right|_{y=0} \tag{1}$$

For air, with the metric system, the temperature variation of viscosity μ can be described by Sutherland's formula for $T \approx 288$ K as

$$\mu = 1.45 \times 10^{-6}\left[T^{\frac{3}{2}}/(T + 110)\right] \sim T^{0.76} \tag{2}$$

The density ρ_∞ is given by

$$\rho = p/(287 \cdot T) \sim 1/T \tag{3}$$

Figure 1 shows a fluid element located next to a flat wall.

In two-dimensional flows, variations in z direction are ruled out by definition. Changes in density and, thus, volume may, therefore, only extend in the x and y direction. Furthermore, if pressure gradients are absent, u_e is constant along x. If density changes were to extend in the x direction also, they would induce changes in u_e, which cannot be counterbalanced by absent pressure gradients. Therefore, density changes induced by wall temperature variations are seen in the y direction only, if pressure gradients are absent.

Thus, for laminar flow, the term $\mathrm{d}u/\mathrm{d}y$ varies with ρ^{-1}, resulting in $\tau_w \sim T^{0.76} \times T^{-1} \sim T^{-0.24}$, which means that, for a flat plate in air without pressure gradients, the surface shear stress (and the Nusselt number) is reduced by increasing the surface temperature.

Table 1 Qualitative change of the local skin-friction coefficient c_f for $Pr = 0.72, M < 1$

	Pressure gradient		
Wall heat transfer	Favorable	Zero	Adverse
Heating	+	——	−
Adiabatic	+	0	——
Cooling	−	+	++

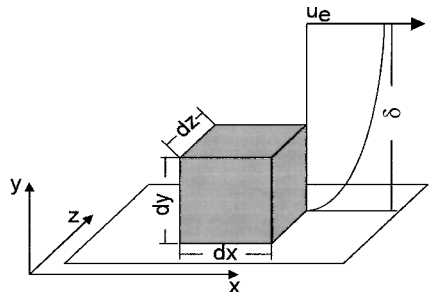

Fig. 1 Finite boundary-layer fluid volume element located adjacent to a surface.

The situation changes, when pressure gradients exist, because they can counterbalance changes in u_e induced by density changes.

Hence, it can be deduced that heat transfer effects on the skin-friction coefficient can be divided in the effect of varying viscosity, which is independent of other influences, and in the effect of density changes, which is enhanced by adverse pressure gradients and diminished by favorable pressure gradients.

Therefore, the effect of varying density leads to an increase of surface shear stress and Nusselt number in favorable pressure gradients when the surface is heated and leads to a reduction in skin friction by heating the surface in adverse pressure gradients. Cooling of the surface leads to a reversal of this effect. The effect of varying viscosity adds to these effects independent of pressure gradients.

The skin-friction coefficient for laminar subsonic flow is, therefore, expected to vary according to Table 1, where a + denotes a weak increase and a ++ a strong increase of the local skin-friction coefficient compared to the adiabatic, zero pressure gradient case and vice versa. These findings agree well with those presented by Morduchow and Grape,[1] as well as with Fig. 10.1 (p. 309) of Cebeci and Bradshaw,[4] among others. For turbulent flows, it is agreed that the specified findings are also qualitatively valid.

These results suggest the use of heat transfer to decrease the drag coefficient c_d by choosing the appropriate heat transfer rates according to the pressure gradient, wherever the expense of a positive or negative heat flux is affordable.

As of immediate interest, the boundary layer around a symmetric NACA 0012 airfoil has been calculated, which incorporates a favorable, a negligible zero and a large slightly adverse pressure gradient region.

III. Calculation Procedure

The drag coefficient c_d is often calculated, and measurements are being made implying the momentum thickness Θ at the trailing edge. This procedure works well for adiabatic flows, but it should not be used here, because heat transfer, especially when nonuniform, leads to density changes and, therefore, changes of the local skin-friction coefficient c_f along the chord length, which cannot be detected from the trailing-edge position. Therefore, an integration of the local skin-friction coefficient c_f should be applied as will be shown to determine the drag coefficient c_d.

The momentum thickness or momentum deficit thickness Θ for coupled boundary layers is given by

$$\Theta = \int_0^\infty \frac{\rho u}{\rho_e u_e}\left(\frac{u_e - u}{u_e}\right) \mathrm{d}y \tag{4}$$

The drag coefficient c_d on a flat plate with surface length l per unit depth is

$$c_d = \frac{1}{l}\int_0^l c_f(x)\,\mathrm{d}x \tag{5}$$

Throughout this contribution, the wall heat flux q''_w is regarded as consisting of a constant value, $|q''_W|$, and a sign. A plus sign denotes constant heat flux from the wall into the boundary layer (wall heating), and a minus sign denotes constant heat flux from the boundary layer into the wall (wall cooling). A plus or minus sign denotes a varying wall heat flux sign along the chord length, resulting in wall heat flux step changes of magnitude $2 \cdot |q''_w|$:

$$q''_w = \mathrm{sgn} \cdot |q''_w| \tag{6}$$

The boundary-layer calculations were carried out applying the numerical method presented by Cebeci and Bradshaw[4] with some minor changes together with an input calculating and data handling tool supplied by the author. The numerical method solves a finite difference representation of the Illingworth–Stewartson transformed boundary-layer variables for laminar and turbulent external flows, applying the Cebeci–Smith turbulence model.

The external velocity distribution was calculated following the method of Hess as presented by Fletcher,[5] with some minor modifications implying the von Kármán–Tsien compressibility correction. An iteration loop to account for the boundary-layer growth was formed calculating the velocity distribution for the displaced flow. This implementation was compared to other implementations of the Hess–Smith method, and it was found that nearly identical velocity distributions were obtained.

IV. Numerical Accuracy

Amick[6] has conducted measurements of the pressure coefficient of a NACA 0012 airfoil. The comparison of these measurements with the calculation method used here are shown in Fig. 2. The agreement of these values is about 1.5%, which is well below the measurement uncertainty. The dimensionless pressure gradient parameter m is included for later reference. It is defined as

$$m = \frac{x}{u_e}\frac{\mathrm{d}u_e}{\mathrm{d}x} \tag{7}$$

The boundary-layer calculation method presented by Cebeci and Bradshaw[4] is complemented by many comparisons to measurements. An additional example is shown in Fig. 3. For this purpose, the local Stanton number, defined as

$$St(x) = \frac{q''_w(x)}{\rho \cdot c_p \cdot [T_w(x) - T_e] \cdot u_e} \tag{8}$$

is calculated. The ratio of the thus obtained Stanton number to the Stanton number for a constant wall temperature indicates the ability

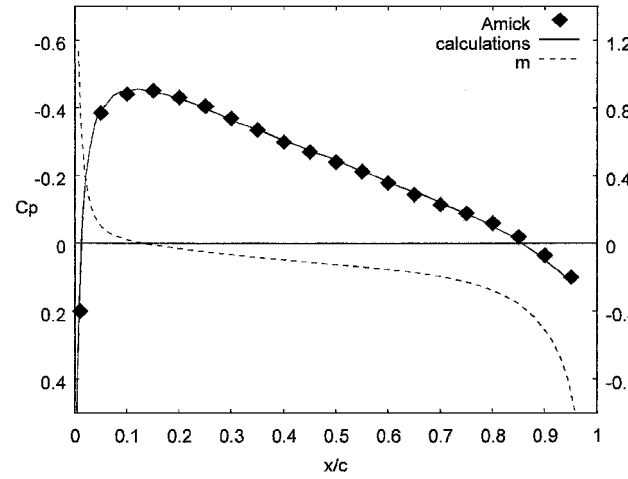

Fig. 2 Current calculations compared to measurements for a NACA 0012 airfoil: measurement data due to Amick[6]; pressure gradient parameter m and $M = 0.4$.

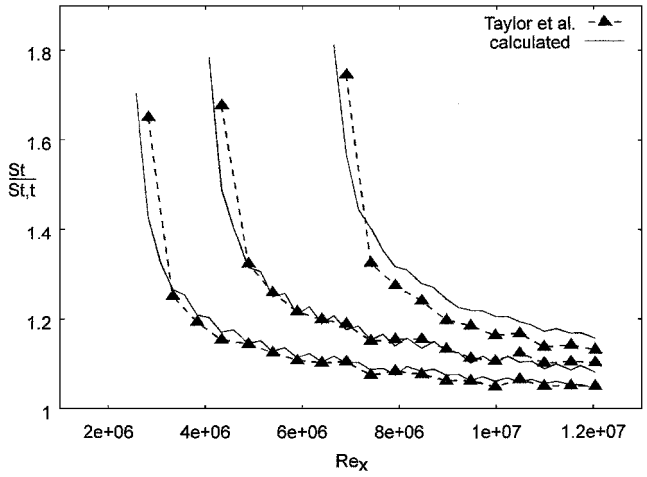

Fig. 3 Unheated starting length Stanton number St normalized by uniformally heated Stanton number St_t for a flat plate; fully turbulent; measurement data due to Taylor et al.[7]: $l = 2.39$ m, $M = 0.19$, $T_0 \approx 305$ K, and $T_h \approx 318$ K. Data used with permission from the American Society of Mechanical Engineers.

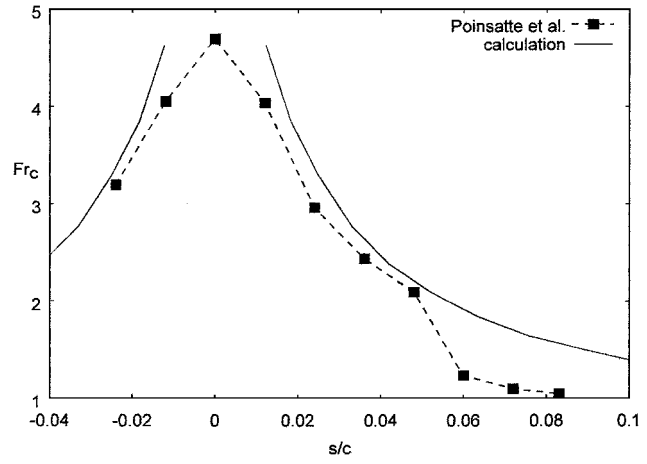

Fig. 4 Leading-edge distribution of Frossling number Fr_c for a NACA 0012 airfoil; measurement data due to Poinsatte et al.[8]: $c = 0.533$ m, $Re_c = 1.19 \times 10^6$, $T_0 \approx 265.9$ K, and $T_h \approx 307$ K.

of the calculation method to resolve step changes in the wall temperature. The Reynolds analogy allows to relate the Stanton number to the skin-friction coefficient.

The flat plate is placed in a uniform stream at $M = 0.191$ with a fully turbulent boundary layer. The initial temperature is $T_0 \approx 305$ K, and the heated region is kept at $T_h \approx 318$ K. The measurement data are due to Taylor et al.[7] Further details and references to the integral solution of this problem are also given in Ref. 7. The calculated values show good agreement over a wide range of x values. Only for the higher Reynolds number Re_x values with the longest unheated starting length, there exists an overprediction by the calculation method. The average calculation uncertainties for the three cases from left to right are 0.31, 1.04, and 2.73%, respectively. The maximum uncertainty is 5.9% for the rightmost case. The average estimated uncertainties given for the measurement data are always more than 2.4%, typically 2.6%.

Measurements of the Frossling number on the leading edge of a NACA 0012 airfoil were conducted by Poinsatte.[8] The Frossling number Fr_c, not to be confused with the Froude number Fr, based on chord is defined as

$$Fr_c = \frac{Nu_c}{Re_c^{0.5}} = \frac{h_c c/k}{(\rho V c/\nu)^{0.5}} \tag{9}$$

The measurements and the calculated values are shown in Fig. 4, with s/c being the surface distance from the leading edge and negative values denoting the pressure side. The calculated values show a good agreement up to $s/c = 0.06$. Poinsatte comments on this unsteadiness as propably being caused by a local surface deformation. Otherwise, again a good agreement of the measured and calculated values can be observed, with a overprediction of 8.1% neglecting the unsteadiness. The qualitative behavior, however, is being accurately modeled by the calculation method.

In conclusion, the accuracy of the numerical method is always better than 8.1%, which can be viewed as good enough to enable qualitatively correct results for the current problem. Some discrepancies especially with Fig. 4 are likely to be due to the measurements.

However, even more important than the accuracy of a single calculation is the numerical accuracy among several calculated values, or relative numerical uncertainty, which determines the validity of derived quantities. It does not relate to the uncertainty compared to the measurements and has to be added to this to obtain overall uncertainties. A high relative numerical uncertainty of subsequent calculations is achievable, when the same calculation grid is used. An estimate for relative numerical uncertainties is given in Sec. VI.

V. Turbulence and Transition

The turbulent-flow calculation is started by activating the eddy-viscosity formulas of the algebraic Cebeci–Smith turbulence model. The details of this model are presented by Cebeci and Bradshaw[4] (see p. 187 and following pages). The accuracy has been found to be sufficient for most engineering problems.

To determine the transition location, the e^n method as given by Cebeci and Cousteix (Ref. 9, p. 196 ff.) has been applied. To include heat transfer effects, the method has been extended by the author following the outline given in Ref. 9, p. 212 and following pages and consists of the solution of the modified Orr–Sommerfeld equation for incompressible flows with heat transfer (see also Wazzan et al.[10]):

$$[(\alpha u - \omega)(\phi'' - \alpha^2\phi) - \alpha u''\phi]i R = \tilde{\mu}(\phi^{iv} - 2\alpha^2\phi'' + \alpha^4\phi) + 2\tilde{\mu}'(\phi''' - \alpha^2\phi') + \tilde{\mu}''(\phi'' + \alpha^2\phi) \tag{10}$$

As discussed by Cebeci and Cousteix (see Ref. 9, p. 188), with the variable flow properties in the preceding equation being supplied by the compressible boundary-layer solution, the method gives also valid results for the airflows considered here.

For the adiabatic case with an n factor of 8.1, good agreement was found among the thus calculated transition location and the location calculated with the empirical formula of Michel[11] (see also Cebeci and Bradshaw,[4] pp. 189–191). In the presence of both heat transfer and pressure gradients, it has been found, for example by Rued and Wittig,[12] that the latter largely dominate the transition to turbulence. Accordingly, the heat flux rates in this contribution were found to have negligible effect on the transition location calculated with the modified e^n method. This finding is not expected to hold for higher heat flux rates or lower Reynolds numbers, but proved reliable for the values considered here. The calculated disturbance frequencies were found to be slightly increased by positive heat flux rates.

Lee[13] presented mesurements and calculations of the laminarization of airfoil boundary layers by heat transfer, where cooling was applied to delay the transition to turbulence. It is reported that, for an aft-loaded FDLA airfoil at a negative angle of incidence, a drag reduction could thus be obtained, but for a NACA 65A413, the drag reduction was much less pronounced. The drag reduction was found to depend on the length of the favorable pressure gradient region, which was extremely long for the first profile and less pronounced for the second one.

VI. Calculations

The calculations were carried out as outlined. Iterations to account for the displacement thickness as well as subiterations to achieve an accurate surface temperature were performed. The turbulence transition location was calculated with the modified e^n method. Freestream values of $T_0 = 288$ K and $p_0 = 101{,}325$ Pa in turbulence-free air ($Pr = 0.72$) for airfoils with a chord length of $c = 1$ m were used except where specified. A heat transfer rate with zero, positive, and negative wall heat fluxes of $q_w'' = \pm 1000$ W/m^2 was chosen to also avoid oscillations of the solution, typical for numerical methods involving (temperature) step changes.

Figure 5 shows results of these calculations for $Re_c = 7.02 \times 10^6$, where the skin-friction factor c_f for uniform surface heat flux rates,

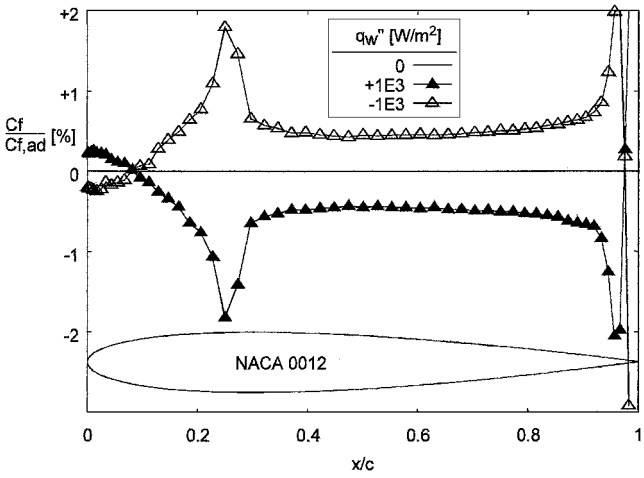

Fig. 5 Relative change of c_f by wall heat transfer compared to the adiabatic wall case: NACA 0012, $Re_c = 7.024 \times 10^6$, and $\alpha_i = 0$.

here constant along the chord length, denoted by $\pm 1E3$, is compared to the adiabatic wall case, denoted by 0 (horizontal line).

The local skin-friction coefficient percentage ratio $c_{f,\mathrm{qw}}/c_{f,\mathrm{aw}}$ (%) shows a change in sign for both heating and cooling at $x/c \approx 0.1$. This is the location where the dimensionless pressure gradient parameter m (see Fig. 2) changes sign from favorable ($m > 0$) to adverse ($m < 0$). The values for positive and negative wall heat flux are nearly exactly opposite to each other, and both show a peak near the turbulence transition location at $x/c \approx 0.28$, which further illustrates the linearity and reliability of the calculation method. The peak near the trailing edge is followed by a sharp decrease. In both cases, separation is indicated at $x/c \approx 0.991$, and the boundary-layer calculation is stopped.

The relative numerical uncertainty relevant for the determination of the drag coefficient reduction has been found to be 0.02% for this case. The overall uncertainty is, therefore, less than 8.2% as determined in Sec. IV.

VII. Drag Coefficient Optimization

Figure 5 confirms the findings in Table 1 that heating the entire airfoil reduces the drag coefficient, and cooling the airfoil increases it, as compared to the adiabatic case, which is well known.

However, it seems to be even more promising to change the temperature gradient sign according to the change of pressure gradient, resulting in a cooled tip region and a heated main part and trailing edge. However, the cooled fluid entering the heated region delays the temperature increase at this location and, hence, the reduction in skin friction. The location of the cooling to heating transition, therefore, needs to be optimized.

To find the optimum heat transfer transition locations, a series of computations with various locations were performed. It was found that the optimum heat transfer transition locations are coupled to the slope of the coefficient of pressure C_p and, hence, to the external flow velocity u_e/u_0 as follows.

Wall cooling:

$$C_p > 0 \equiv u_e/u_0 < 1 \Rightarrow q_w'' < 0$$

Wall heating:

$$C_p < 0 \equiv u_e/u_0 > 1 \Rightarrow q_w'' > 0$$

Applying this simple rule, the velocity distribution with heat transfer (curved dotted lines) along the similar boundary layer distance η (y direction) compared to the adiabatic wall case (straight lines) is shown in Fig. 6. For better visibility, the x location of the velocity profiles in Fig. 6 is scaled using an arbitrary scaling factor of $N = 5$:

$$x = x/c + [(u_{\mathrm{qw}}/u_{\mathrm{aw}}) \cdot N] - N$$

The thermal efficiency η_{th} (not to be confused with the similar boundary-layer distance η) is calculated according to

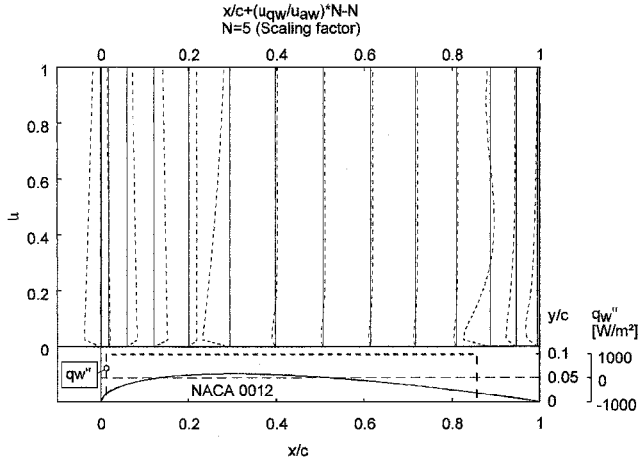

Fig. 6 Heat transfer induced changes of the velocity distribution across the boundary layer compared to the adiabatic velocities: NACA 0012, $\alpha_i = 0$, $q_w'' = \pm$ 1000 W/m², and $Re_c = 7.024 \times 10^6$.

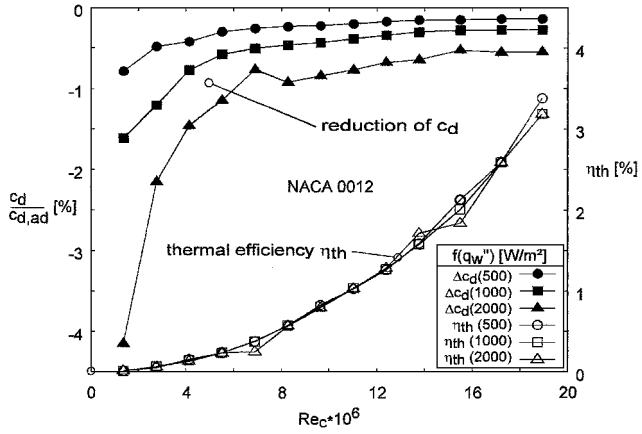

Fig. 7 Drag reduction by heat transfer; thermal efficiency η_{th} with chord Reynolds number Re_c: NACA 0012; $q_w'' = \pm$ 500, 1000, and 2000 W/m²; and $\alpha_i = 0$.

$$\eta_{\mathrm{th}} = \frac{W_{D,\mathrm{aw}} - W_{D,\mathrm{qw}}}{q_{w,\mathrm{abs}}} \tag{11}$$

The wall heat rate $q_{w,\mathrm{abs}}$ (watt) per unit depth is formed from the wall heat flux q_w'' (watt per square meter) as follows, with x_s being the surface distance:

$$q_{w,\mathrm{abs}} = \int_0^{x_s} |q_w''| \, \mathrm{d}x \tag{12}$$

The drag work W_d is

$$W_d = 0.5\rho_0 u_0^3 A \cdot c_d = 0.5\left[\mu_0^3 \Big/ \left(c^3 \rho_0^2\right)\right] \cdot Re_c^3 \cdot A \cdot c_d \tag{13}$$

VIII. Discussion of the Results

Figure 7 shows the resulting optimum attainable reduction of the drag coefficient with chord Reynolds number Re_c corresponding to freestream Mach numbers ranging from 0.07 to 0.8 for $q_w'' = \pm 500$, 1000, and 2000 W/m², denoted by $c_{d,\mathrm{qw}}$ together with the corresponding thermal efficiency η_{th}.

The maximum relative numerical uncertainty is 34.8%; the average uncertainty is 7.5% in this case. In the observed velocity range, the turbulence transition locations move swiftly upstream with increasing velocity. Because of the finite grid spacing, the movement is stepwise, occurring at $Re_c = 6.8$ and 13.77×10^6, which explains the deviating values there. If these values were omitted, the maximum uncertainty is 19%, and its average is 3.6%.

The course of the drag coefficient reduction exhibits a dependence on q_w'', which the course of η_{th} together with Fig. 5 suggest as being linear. The course of η_{th}, thus, is independent of q_w'' and only depends

on the chord Reynolds number Re_c for the given conditions (NACA 0012, $c = 1$ m, $\alpha_i = 0$, and $M < 1$) as follows:

$$\eta_{\text{th}} \approx Re_c^2 \cdot c_{ht} \quad \text{where} \quad c_{ht} = 9.1 \times 10^{-17} (\cdot 100 \text{ for } \eta_{\text{th}},\ \%) \tag{14}$$

The factor c_{ht} is an empirical curve fit parameter and is introduced for convenience. Relating η_{th} to the Reynolds number is preferred over the Mach number because the former relates inertia to viscous effects, which appears to be more adequate for the current problem. The average uncertainty of c_{ht}, determined from the values given earlier for the relative numerical uncertainty when the two deviating values are omitted, together with the measurement uncertainties from Sec. IV, is 11.7%.

The value of c_{ht} surely is problem dependent. A regular dependency could be assumed; for example,

$$c_{ht} = f\left(\frac{\mathrm{d}p}{\mathrm{d}x}; \alpha_i; \frac{\mathrm{d}q''_w}{\mathrm{d}x}; Pr; C \ldots\right) \tag{15}$$

with C denoting the Chapman–Rubesin viscosity law defined as $C = \rho_w \mu_w / \rho_e \mu_e$. However, further investigations are necessary to identify the influences of these terms. For the drag reduction, it follows from Eqs. (11) and (14) that

$$c_{d,\text{aw}} - c_{d,\text{qw}} = c_{ht} \cdot \frac{q_{w,\text{abs}} \cdot c}{0.5A \cdot Re_c \cdot \mu_0} \tag{16}$$

or, normalized by the drag coefficient for the adiabatic wall case $c_{d,\text{aw}}$,

$$\frac{c_{d,\text{qw}}}{c_{d,\text{aw}}} = 1 - \frac{c_{ht}}{c_{d,\text{aw}}} \cdot \frac{q_{w,\text{abs}} \cdot c}{0.5A \cdot Re_c \cdot \mu_0} \tag{17}$$

which is also shown in Fig. 7. For constant $q''_w = q_{w,\text{abs}}/A$, of course, this cancels against A. The generally low value of η_{th} determines that the prescribed method is suitable for drag reduction wherever heat or coldness is freely or cheaply available.

IX. Comparison with Previous Investigations

The already mentioned theoretical ideal flow investigation by Oswatitsch[2] and the measurements of Feltgen[3] (see Sec. I) lead to the findings that heating the freestream by externally burning (hydrogen) gas at the leading and the trailing edges of an airfoil generates thrust. Thus, the (subsonic) heat transfer locations are identical with those found herein; however, the heat flux sign is opposite. This disagreement with the presented results needs to be clarified. The significant difference is the ideal flow assumption (external heating), affecting the pressure distribution, compared to the boundary-layer approach (wall heating) affecting the wall shear stress.

Note that, observed from a position inside the boundary layer, the freestream is on one side ($\eta \to \infty$) and the wall is on the opposite side ($\eta \to 0$). Therefore, it is clear that, in terms of the boundary-layer heat flux, heating the freestream flow, that is, $\eta \to \infty$, at a certain x/c location corresponds to cooling the wall, that is, $\eta \to 0$, at the same x/c location.

Mathematically, both cases correspond to an interchange of boundary conditions, which will result in an interchange of the behavior of the layer, now illustrating the agreement between Oswatitsch,[2] Feltgen,[3] and the boundary-layer behavior described here.

X. Examples

From the preceding results, two degenerate cases of the prescribed method, which appear more convenient for practical purposes, can be deduced. The first case consists of cooling the tip of the airfoil up to the first heat transfer transition location, adiabatic wall heat flux up to the second location, and cooling again downstream up to the trailing edge. The second case conversely consists of heating the wall in between the two transition locations and keeping the leading and the trailing edge adiabatic.

As a first example, a NACA 2412 airfoil with chord length $c = 0.1$ m is examined, which can be interpreted as a simplified representation of the situation found at a gas turbine blade. The external temperature is $T_0 = 1523$ K, the chord Reynolds number is 1.38×10^6, and the pressure is $p_0 = 10$ bar.

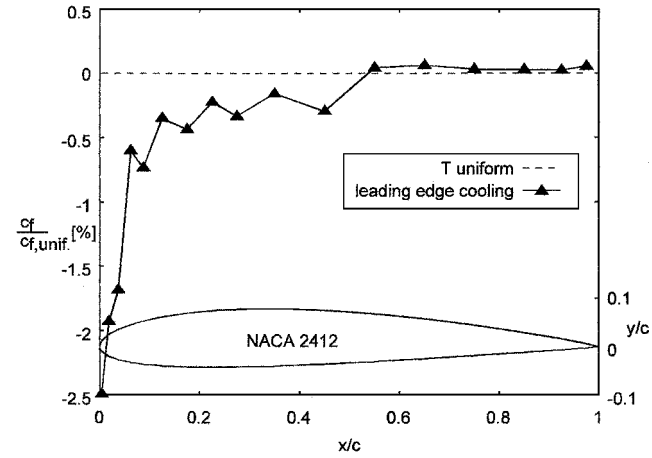

Fig. 8 Reduction of the local skin-friction coefficient c_f; improved cooling at the leading edge vs uniform cooling: NACA 2412, $\alpha_i = 0$, $T_0 = 1523$ K, $p_0 = 10$ bar, $Re_c = 1.38 \times 10^6$, and $T_s = 1123$ K.

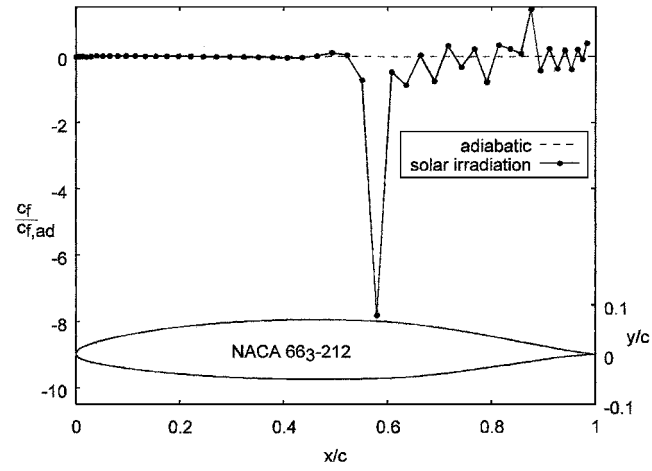

Fig. 9 Reduction of the local skin-friction coefficient c_f for a NACA 66_3–212 airfoil at zero angle of attack with solar irradiation and varying absorption coefficient.

The surface temperature is initially kept uniformly at $T_s = 1123$ K because cooling is vitally important to decrease the thermal strain of the material. However, it was found that this isothermal cooling already carries a penalty in terms of a drag coefficient increase of 6.2% compared to the adiabatic case.

To achieve a reduction of this drag coefficient penalty, the blade cooling is now improved by any means from the leading edge to the first heat transfer transition location, occurring at $x/c \approx 0.037$, from where it remains unchanged until the trailing edge. Improved cooling is implemented by specifying a constant surface temperature of $T_s = 1023$ K, while the remainder of the surface is again kept at $T_s = 1123$ K.

Figure 8 shows the percentage of reduction of the skin-friction coefficient c_f by improved cooling of the leading edge, compared to the constant surface temperature case as specified earlier, along the chord length. The reduction of the drag coefficient c_d integrates to give 0.52%. The relative accuracy is again 0.02%. In this case, no significant effect of a second transition location, which was found to occur at $x/c \approx 0.975$, that is, near the trailing edge, could be determined, which may be due to the specific calculation setup as already mentioned and not necessarily to the physics of this case.

Further improvements in drag coefficient reduction can of course be achieved by further decreasing the surface temperature near the leading and, with less effect, near the trailing edge, or by increasing T_s at the rest of the geometry.

As another example, the effect of heating the upper surface of a NACA 66_3–212 airfoil by solar irradiation in conjunction with varying the absorption coefficient (absorptivity), along the chord length from 0 (white) to 1 (black) is examined. Figure 9 shows the airfoil

geometry, where the chord length is $c = 1$ m, together with the local skin-friction coefficient reduction achieved for $Re_c = 6.8 \times 10^6$. This airfoil type has a prolonged laminar section, thus already designed for low skin-friction drag. However, it does not possess an extremely long favorable pressure gradient section as an aft-loaded FDLA airfoil.

The optimum heat transfer transition locations were found to occur at $x/c \approx 0.03$ and 0.975. The solar irradiation was assumed to be $q''_{w,\mathrm{sol}} = 676.5$ W/m^2. Only the upper surface is irradiated, the lower surface remains adiabatic. The variation of the surface orientation was acccounted for by a cosine relationship. The resulting reduction of the drag coefficient c_d is 0.28%, which may be expected to vary with Reynolds number Re_c according to Fig. 7. The numerical relative uncertainty is 0.02%. The negative spike in Fig. 9 occurs at the location of the transition to turbulence, slightly downstream from the location where the pressure gradient becomes adverse.

Actually integrating over the solar spectrum does not lead to a black surface for optimum heat absorption but rather to a greenish colour. To achieve a maximum heat transfer rate, blackbody behavior is necessary, and so the actual optimum color needs to be computed for a given configuration, which is beyond the scope of this contribution.

XI. Conclusions

It was shown by numerical calculations how heat transfer variations can be used to reduce the skin-friction drag, occurring at airfoil-like geometries. An empirical dependancy of the drag reduction and the thermal efficiency on the squared Reynolds number could be established. The drag reduction is proportional to the heat flux, whereas the thermal efficiency only depends on the Reynolds number. The thermal efficiency is generally low. The drag reduction can reach interesting values by increasing the heat flux. Two illustrative examples with varying heat flux distribution and geometry were presented and considered in detail.

Several different methods for obtaining reductions of the drag coefficient have been reported on in the past. The method reported on here does not stand in direct competition with these methods. It can make use of exhaust gases, turbine bleed air, heat exchangers or merely solar irradiation, which are available cheaply and are otherwise lost, to help increasing the overall efficiency of many different technical devices. The design of aerothermal systems such as turbine blades gains additional information on avoiding excessive losses when following the guidelines established in the course of this contribution.

Acknowledgments

The support of T. Cebeci and J. P. Shao concerning the modifications to the e^n calculations is greatly appreciated. The author would also like to acknowledge the courses held by J. Katz, O. Knio, and C. Meneveau from the Johns Hopkins University, Baltimore, Maryland.

References

[1]Morduchow, M., and Grape, R. G., "Separation, Stability, and other Properties of Compressible Laminar Boundary Layer with Pressure Gradient and Heat Transfer," NACA TN 3296, 1955.

[2]Oswatitsch, K., "Antriebe mit Heizung bei Überschallgeschwindigkeit," Deutsche Versuchsanstalt für Luftfahrt, Rept. 90, Westdeutscher Verlag, 1959.

[3]Feltgen, K., "Widerstandsverringerung umströmter Körper durch Verbrennung in ihrem Staugebiet," Ph.D. Dissertation, Technische Hochschule München, Munich, 1962.

[4]Cebeci, T., and Bradshaw, P., *Physical and Computational Aspects of Convective Heat Transfer*, Springer, Berlin, 1984, pp. 187, 189–197, 309.

[5]Fletcher, C. A. J., *Computational Techniques for Fluid Dynamics*, Vol. 2, Springer, Berlin, 1991, pp. 130–144.

[6]Amick, J. L., "Comparison of the Experimental Pressure Distribution on an NACA 0012 Profile at High Speeds with that Calculated by the Relaxation Method," NACA TN 2174, 1950.

[7]Taylor, R. P., Love, P. H., Coleman, H. W., and Hosni, M. H., "Heat Transfer Measurements in Incompressible Turbulent Flat Plate Boundary Layers with Step Wall Temperature Boundary Conditions," *Journal of Heat Transfer*, Vol. 112, 1990, pp. 245–247.

[8]Poinsatte, P. E., "Heat Transfer Measurements from a NACA 0012 Airfoil in Flight and in the NASA Lewis Icing Research Tunnel," NASA CR 4278, 1990.

[9]Cebeci, T., and Cousteix, J., *Modeling and Computation of Boundary-Layer Flows*, Horizons, Long Beach, CA, and Springer, Berlin, 1999, p. 188 ff.

[10]Wazzan, A. R., Okamura, T., and Smith, A. M. O., "The Stability of Water Flow Over Heated and Cooled Flat Plates," *Journal of Heat Transfer*, Vol. 90, 1968, pp. 109–114.

[11]Michel, R., "Etude de la Transition sur les Profiles d'Aile; Établissement d'un Critère de Détermination de Point de Transition et Calcul de la Trainée de Profile Incompressible," ONERA, Rept. 1/157A, 1951.

[12]Rued, K., and Wittig, S., "Laminar and Transitional Boundary Layer Structures in Accelerating Flow with Heat Transfer," *Journal of Turbomachinery*, Vol. 108, 1986, pp. 116–123.

[13]Lee, J. D., "The Influence of Heat Transfer on the Drag of Airfoils," NASA Rept. AD-A098822, 1981.

P. R. Bandyopadhyay
Associate Editor